NINTH EUROPEAN ROTORCRAFT FORUM

Paper No. 51

FREE-VIBRATION ANALYSIS OF A DARRIEUS WIND TURBINE BLADE

F. NITZSCHE

Instituto de Atividades Espaciais

(São José dos Campos)

BRAZIL

September 13-15, 1983

STRESA , ITALY

Associazione Industrie Aerospaziali

Associazione Italiana di Aeronautica ed Astronautica

FREE-VIBRATION ANALYSIS OF A DARRIEUS WIND TURBINE BLADE

Fred Nitzsche
Instituto de Atividades Espaciais
BRAZIL

Abstract

The free-vibration problem of a Darrieus vertical axis wind turbine blade is studied in detail. The transfer matrix method, linked to an integrating matrix scheme, is used for the first time to analyze the three-dimensional eigenvalue problem. The physical model includes distributed properties of both inertia and stiffness, different types of blade support, static unbalance, rotary inertia, and also some degree of both extensibility and shear deformation of the cross section of the blade. The analysis demonstrates the fundamental role played by the Coriolis force and how two simple fundamental modes of the structure are coupled by the same rotational effect and develop a complex free-vibration motion.

Nomenclature

A	area of the blade cross section
a_i	dimensionless structural parameters (Appendix)
b	blade semichord
$\underset{\sim}{C}$	Coriolis matrix
E	Young's modulus
EA	axial stiffness
EI_i	bending stiffness ($i = x, y$)
$\underset{\sim}{F}$	matrix of external loads
$\underset{\sim}{f}_u, \underset{\sim}{f}_v, \underset{\sim}{f}_w$	component of the Coriolis force
$\underset{\sim}{G}, \underset{\sim}{G}_{cor}$	coefficient matrices in the Laplace domain (Eqs. 9, 13)
G	shear modulus
GA	shear stiffness
GI_α	torsional stiffness
$\underset{\sim}{H}$	coefficient matrix in the Laplace domain (Eq. 1)
$\underset{\sim}{K}_D$	dynamic stiffness matrix
$\underset{\sim}{L}$	integrating matrix
ℓ	total length along s-coordinate
$\underset{\sim}{M}$	mass matrix
M_i	component of the internal bending moment of the blade ($i = 1,2$)
M_3	component of the internal torque
O,O'	origin of the reference frame of the cross section; undisturbed position, pertubed position
p	Laplace variable
Q_i	component of the resultant shear force at the blade cross section ($i = 1,2$)
r_α	radius of gyration of the cross section
S,S'	shear center; undisturbed, perturbed position
s	spatial coordinate along the blade
$\underset{\sim}{T}$	transfer matrix
$\underset{\sim}{T}_R$	reduced transfer matrix
t	time

u, v, w	local linear displacement of the elastic axis
$\dot{\underset{\sim}{u}}, \dot{\underset{\sim}{v}}, \dot{\underset{\sim}{w}}$	component of the relative velocity of the elastic axis in the u, v, w directions
x, y	coordinate fixed to the blade
x_α	dimensionless position of the center of mass of the blade cross section in semichords (Fig. 4)
$x^{(n)}$	dimensionless position of the neutral center of the blade cross section in semichords (Fig. 4)
$\underset{\sim}{Y}$	local state vector
$\underset{\sim}{Z}$	coefficient matrix containing structural terms

Greek Symbols

α	torsion of the blade cross section
θ	azimuth angle of the blade
$\kappa^{(o)}$	local curvature of the troposkien
λ	dimensionless group (Appendix)
$\underset{\sim}{\rho}$	vector defining the position of the center of mass of the blade cross section
σ	density of the material of the blade
τ, τ_{max}	local tension, maximum local tension on the troposkien
ϕ	local angle of the troposkien (Fig. 2)
χ_i	rotation of the cross section (i = 1,2)
$\underset{\sim}{\Omega}$	absolute angular velocity vector of the blade
Ω	spinning rate of the turbine
ω	harmonic frequency
ω_i	eigenfrequency i

Other Symbols

$\dot{(\ )}$	time differentiation
$(\ )_{,\theta}$	azimuth angle differentiation

$(\bar{\ })$	dimensionless quantity
$(\ )^*$	state vector extension of a matrix originally relating only forces to displacements
$^*(\ )$	characteristic value (eigenvalue)
$(\underset{\sim}{\ })$	matrix or vector
$(\ )^{-1}$	inverse matrix
$(\ )^T$	transpose matrix
$\langle\ \rangle$	diagonal matrix
$(\ )_D$	displacement subset
$(\ )_F$	force subset
$(\ )_H$	horizontal (radial) component of a vector
$\underset{\sim}{0}$	null matrix
$\underset{\sim}{1}$	unit matrix
j	$\sqrt{-1}$

1. Introduction

The Darrieus rotor belongs to the class of vertical axis turbines used to generate electric power from the wind (Fig. 1). The particular characteristics of the Darrieus rotor have been challenging analysts in the fields of aerodynamics and structural dynamics. Accidents reported with some of these turbines have indicated that much improvement must be done on the existing theory so that the new generation of large and more economical machines may be considered fully reliable. The troposkien shape has been sometimes invoked in structural modeling of the blades of the Darrieus rotor. When gravity effects are neglected, the troposkien can be seen as the plane curve described by a rope rotating at a constant spinning rate. Its shape is known in closed analytic form[1]. A blade with such geometry is characterized by having no bending stress in the equilibrium position determined by a constant angular velocity. However, a three-dimensional vibration pattern develops as soon as the blade is disturbed from its troposkien equilibrium. The resultant motion involves

in-plane (flatwise) and out-of-plane (chordwise) bending of the structure as well as torsion. The aeroelastic stability of the Darrieus turbine with troposkien geometry has been studied in few theoretical works[2,3,4]. The tendency among investigators is to deal with a more general geometry and to use the finite element method in the analysis [5,6,7]. However, the actual shape of Darrieus turbines is very close to the troposkien[8]. The purpose of this work is to present a semi-analytical theory based upon the troposkien approximation which is useful not only to understand the physical phenomena but also to provide data for flutter-type stability analyses.

The geometric properties of the turbine analyzed in this work are those of an actual vertical wind turbine a 17-meter Darrieus turbine manufactured by Alcoa and originally designed by the Sandia Laboratories of New Mexico to generate 70 kilowatts of electric power. A larger 42-meter model of this turbine collapsed during tests in Southern California Edison's facilities in 1981. The properties of the blade are summarized in Table 1. In this machine the blades are unstrutted, according to a new aerodynamically more efficient design[9].

2. Free-vibration Governing Equations

The free-vibration equations governing the motion of small pertubations from the troposkien equilibrium position, connected to both the displacement of the elastic axis of the blade and the corresponding rotations associated with the deformations of the cross section were derived in previous works[10,11].

These equations are linear and include the most important parameters that may affect the analysis, such as CG offset and rotary inertia. Also, some degree of shear deformation and extensibility of the structure is allowed.

Figures 2, 3 and 4 define the parameters involved in the analytical formulation of the problem. The free-vibration governing equations are repeated in the Appendix for the sake of completeness.

3. A Transfer-Integrating Matrix Scheme to Solve Eigenvalue Problems

An efficient approach to the solution of dynamic problems related to free and forced vibration of one-dimensional structures was discussed in detail in a previous work[12]. The new method combines the classical transfer-matrix method[13] with a numerical scheme derived from the theory of integrating matrices[14].

According to the same scheme, integrating matrices are used to derive transfer matrices of the structure. Summarizing the method, the governing equations of motion of the system are first written in state vector form:

$$\frac{d}{ds}\,\underset{\sim}{y} = \underset{\sim}{H}(s;p)\,\underset{\sim}{y} \tag{1}$$

where

$$y = \{\underset{\sim}{y}_F \underset{\sim}{y}_D\}^T \tag{2}$$

and then discretized with respect to the independent variable s. In general, the matrix $\underset{\sim}{H}(s;p)$ contains both structural equilibrium relations and external loads acting on the system. The external loads are Laplace transformed to eliminate the time dependence:

$$\underset{\sim}{H}(s;p) = \underset{\sim}{Z}(s) + p^2\underset{\sim}{M}^*(s) + p\underset{\sim}{C}^*(s) + \underset{\sim}{K}_D{}^*(s) + \underset{\sim}{F}^*(s;p) \tag{3}$$

where $\underset{\sim}{M}^*$, $\underset{\sim}{C}^*$ and $\underset{\sim}{K}_D{}^*$ are respectively the mass, Coriolis and dynamic stiffness matrices of the system; $\underset{\sim}{Z}(s)$ is the matrix containing structural equilibrium terms and $\underset{\sim}{F}^*$ is a matrix of external forces of non-dynamic origin. Pre-multiplying Eq.(1) by an integrating matrix $\underset{\sim}{L}$ and rearranging the expression, one gets:

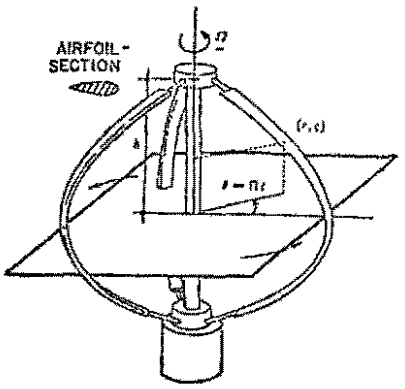

Fig.1: Darrieus rotor

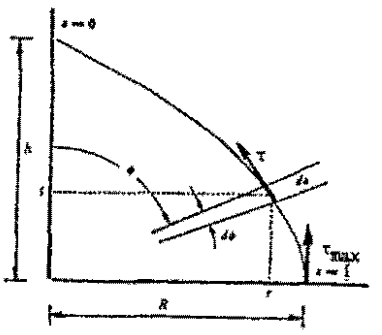

Fig.2: Troposkien definitions

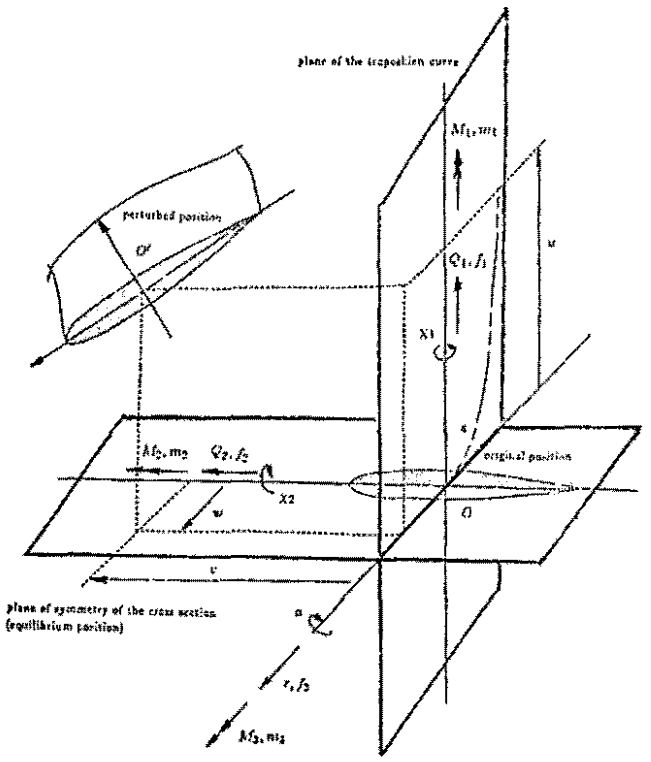

Fig.3: Perturbation Field. Single arrows represent forces. Double arrows represent moments. Observe the original and perturbed positions of the cross section. All quantities are measured in the frame of reference defined by the undisturbed position of the blade.

Fig.4: Blade cross section: definitions. x_α specifies the position of the center of mass in units of semichord (measured from the elastic axis and positive as indicated).

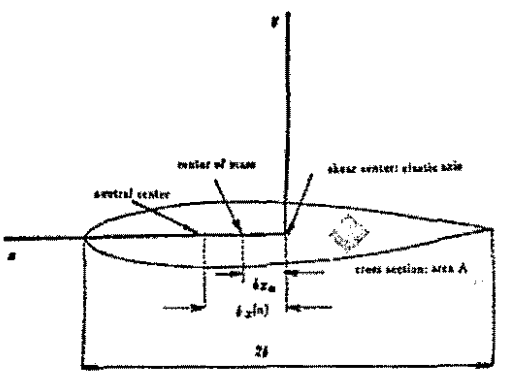

$$\underline{y} = (\underline{\underline{1}} - \underline{\underline{L}}\underline{\underline{H}})\underline{y}_1 \qquad (4)$$

where $\underline{y}_1$ is the state vector evaluated at the end point considered as initial in the process of numerical integration. It is analogous to the constant of integration in exact problems.

From Eq.(4), by simple inspection, all transfer matrices of the one-dimensional structure are obtained and in particular one relating the extremes of the integration path. These are also the end points of the structure:

$$\underline{y}_n = \underline{\underline{T}}(p)\underline{y}_1 \qquad (5)$$

By applying the boundary conditions and consequently eliminating half of the lines and columns in Eq.(5), the characteristic values of the system are determined:

$$|\underline{\underline{T}}_R(^*p)| = 0 \qquad (6)$$

where $\underline{\underline{T}}_R$ is the reduced transfer matrix of the system between the two end points and $^*p$ is an eigenvalue. Eigenvectors are then obtained by successively solving Eq.(4) with $^*p$ for the intermediate transfer matrices. Examples of application of this technique in some classical eigenvalue problems are presented in Ref. 12. In the same work accuracy of the method is tested. Throughout this work the characteristic values of Eq.(6) will be obtained via a root finder routine based upon Muller's method to calculate complex roots of analytical functions[15]. Once the convergence to a complex root is acheived, its complex-conjugate pair is automatically eliminated by the algorithm to avoid unnecessary searches. The integrating matrix employed in the integrating scheme is based on a 5th. order Newton's forward-difference formula and may be found in Ref. 11. A complete table of integrating matrices is presented in Refs. 14 and 16. The results in

Sects. 4 and 5 were obtained by taking 11 discretizating points along the structure.

4. Free-Vibration Eigenvalue Problem with no Coriolis Effect

When the Coriolis-related matrix is subtracted form the dynamic load, the free-vibration eigenvalue problem in state vector form is written as:

$$\frac{d}{ds}\underset{\sim}{y} = \underset{\sim}{Z}\underset{\sim}{y} + \underset{\sim}{M}^*\ddot{\underset{\sim}{y}} + \underset{\sim}{K}_D^*\underset{\sim}{y} \tag{7}$$

Taking the Laplace transform of Eq.(7), time is eliminated from the equation of motion yielding:

$$\frac{d}{ds}\underset{\sim}{y} = \underset{\sim}{G}(s;p)\underset{\sim}{y} \tag{8}$$

where

$$\underset{\sim}{G}(s;p) = \underset{\sim}{Z}(s) + p^2\underset{\sim}{M}^*(s) + \underset{\sim}{K}_D^*(s) \tag{9}$$

The dimensionless matrices that appear in Eq.(9) are repeated from Ref. 11 and presented in the Appendix. The eigenvalue problem is then solved by closely following the procedure explained in Sect. 3. Here, the matrix $\underset{\sim}{G}$ replaces the matrix $\underset{\sim}{H}$ in Eq.(1). As formulated, the non-dimensionalized eigenvalues are obtained as pure imaginary numbers since no structural damping is assumed:

$$^*\overline{p} = \frac{\omega}{\Omega}j \tag{10}$$

where ω is the natural frequency and Ω is the magnitude of the absolute angular velocity vector of the blade. As long as there is no Coriolis effect, the characteristic of the sistem is such that all eigenvectors are real vectors. The orthogonality property holds and eigenvectors related to different eigenvalues are orthogonal.

Figure 5 shows the behavior of the first two

natural frequencies when the angular velocity of the turbine is changed. Pinned joints are assumed at both ends. In analogy with the free vibration of a string, the natural frequencies of the troposkien blade are heavily dependent upon the turbine's spinning rate, which directly affects the tension on the blade. In Fig. 6 the ratio of the same two frequencies is plotted against the turbine's rpm and one notices that the separation between these two eigenfrequencies decreases as the spinning rate increases.

The corresponding eigenvectors for the first two natural frequencies of the blade are plotted in Figs. 7 and 8. Aside from some minor differences, the shape of the eigenvectors remains constant within the operational range of the turbine, between 20 and 50 rpm. Normalization is made with respect to their largest component. In Fig. 7 the case is considered in which there is no static unbalance and so the center of mass coincides with the shear center of the cross section of the blade. The second case, in Fig. 8, is an example in which the center of mass is moved towards the trailing edge of the airfoil by a tenth of the blade semichord. (x_α = -0.1, according to Fig. 4).

From the former situation it becomes clear that when there is no center of mass offset the first natural mode consists of an antisymmetric flatwise bending (motion of the elastic axis in the u-direction) combined with a symmetric spanwise displacement of the structure (displacement in the w-direction). As a remark, the latter should not be regarded as a stretching of the blade, which contribution on the results is evidently secondary. The second natural mode is a combination of antisymmetric torsion and chordwise bending of the blade (motion of the elastic axis in the v-direction). One should also stress that the absence of a symmetric flatwise first mode with

nodes only at both ends of the structure is indeed expected due to the particular distribution of curvature which characterizes the troposkien.

In The latter situation of Fig. 8, a coupling between torsion and flatwise bending is already noticed. Such coupling is still small for this value of the center of mass offset parameter, but larger values of x_α are uncommon.

In Fig. 9 an example in which clamped joints are used is presented. For a close comparison with the previous example, the center of mass was also set at the position $x_\alpha = -0.1$. The first natural mode is similar in shape to its equivalent with pinned joints. However, the chordwise bending component is one order of magnitude lower, as a result of imposing a more restraining boundary condition. The most interesting difference between the two latter examples comes with the second natural mode, which now consists of an almost pure symmetric chordwise bending of the blade. The amplitude of the torsion component of the eigenvector is one order of magnitude lower and has a symmetric shape with two intermediate nodes. As expected, the eigenfrequencies are higher in the clamped than in the pinned joints case, following the lateral free-vibration characteristics of a straight beam.

5. Complete Free-Vibration Eigenvalue Problem

When Coriolis effect is included, the free-vibration eigenvalue problem in state vector form reads:

$$\frac{d}{ds}\underline{y} = \underline{Z}\underline{y} + \underline{M}^*\ddot{\underline{y}} + \underline{C}^*\dot{\underline{y}} + \underline{K}_D{}^*\underline{y} \qquad (11)$$

Likewise in Sect. 4, time is eliminated by Laplace transforming Eq. (11):

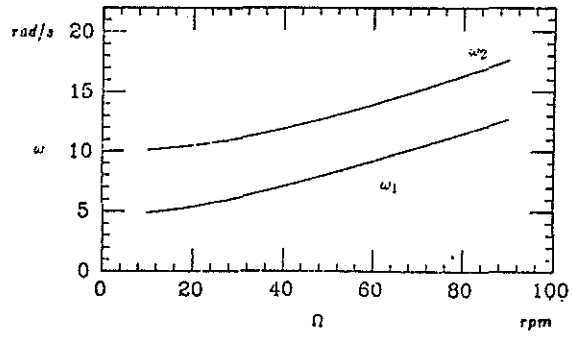

Fig.5: First two natural frequencies as function of the spinning rate. No Coriolis effect is included. Pinned joints and $x_\alpha = 0$.

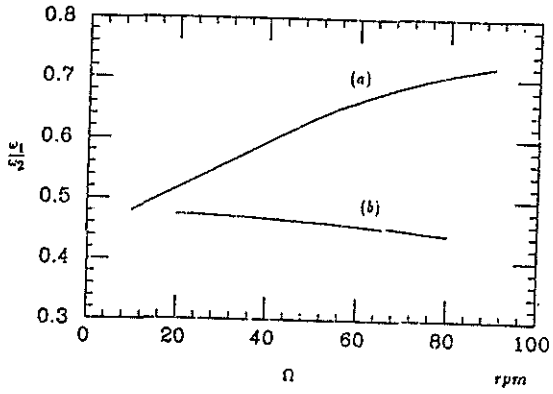

Fig.6: Ratio of the first two natural frequencies as function of the spinning rate. (a) is obtained without Coriolis effect, whereas (b) includes it. Conditions as Fig. 5.

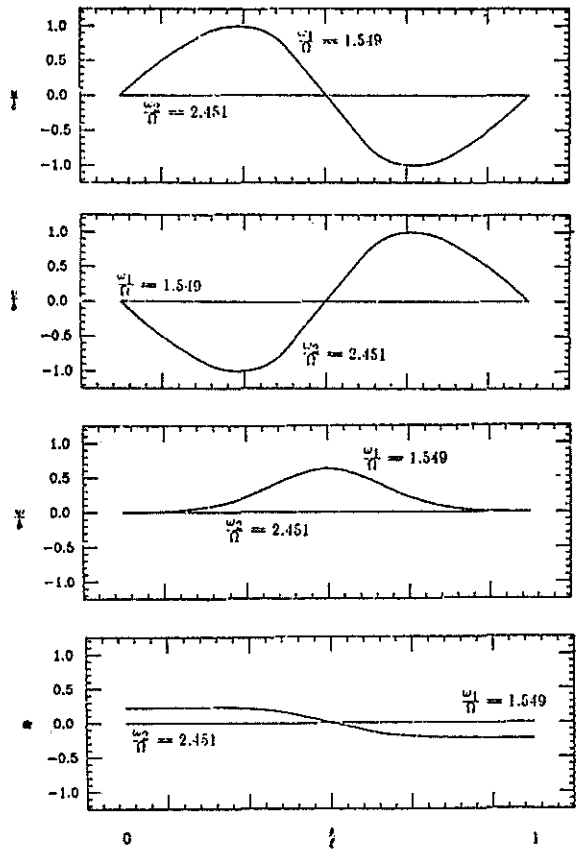

Fig.7: First two eigenvectors of the case without Coriolis computed at 50 rpm. The components, from top to bottom: flatwise bending, chordwise bending, spanwise displacement and torsion. Pinned joints and $x_\alpha = 0$.

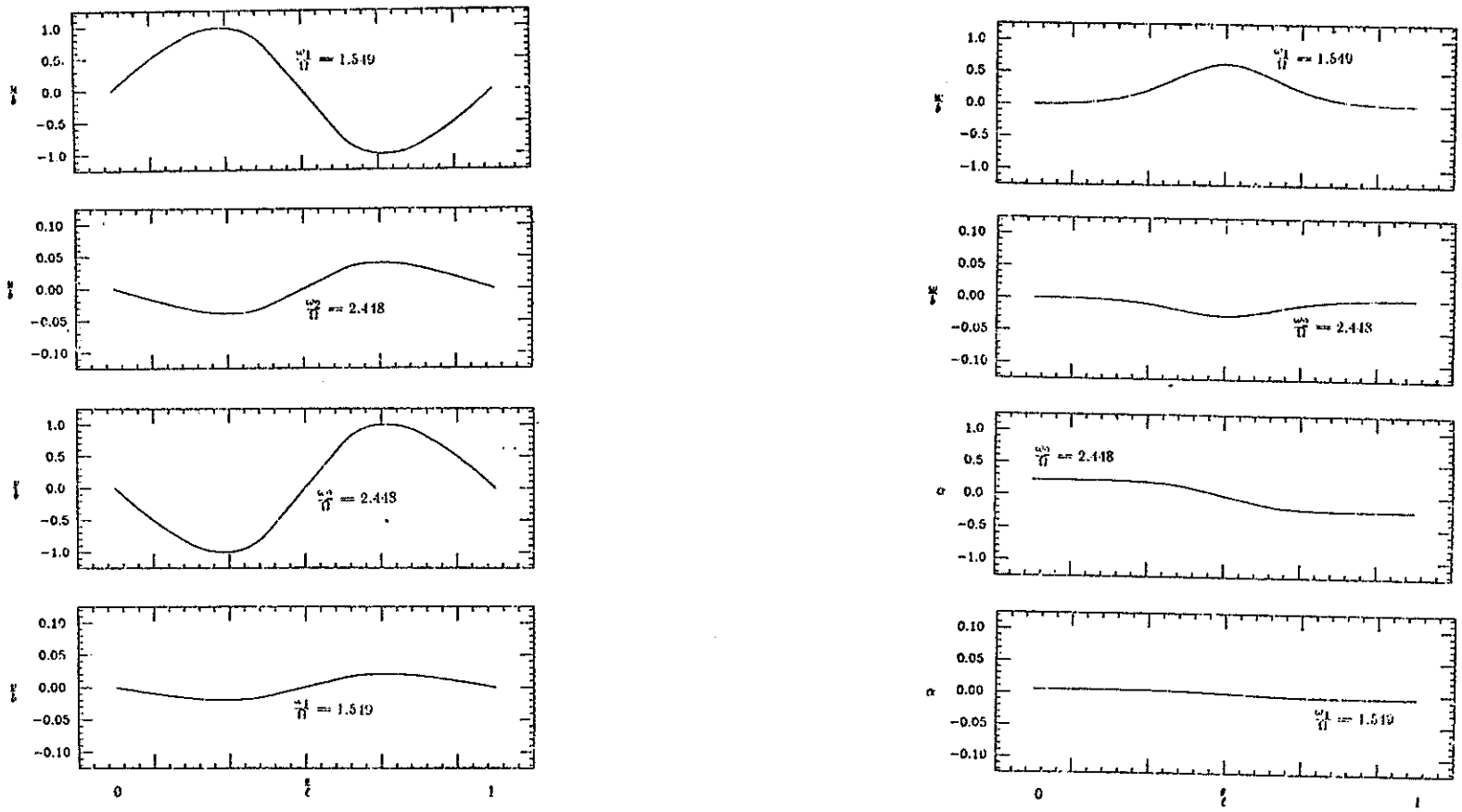

Fig.8: First two eigenvectors of the case without Coriolis computed at 50 rpm. The components, from left to right and from top to bottom: flatwise bending, chordwise bending, spanwise displacement and torsion. Observe different scales in each situation. Pinned joints and $x_\alpha = -0.1$.

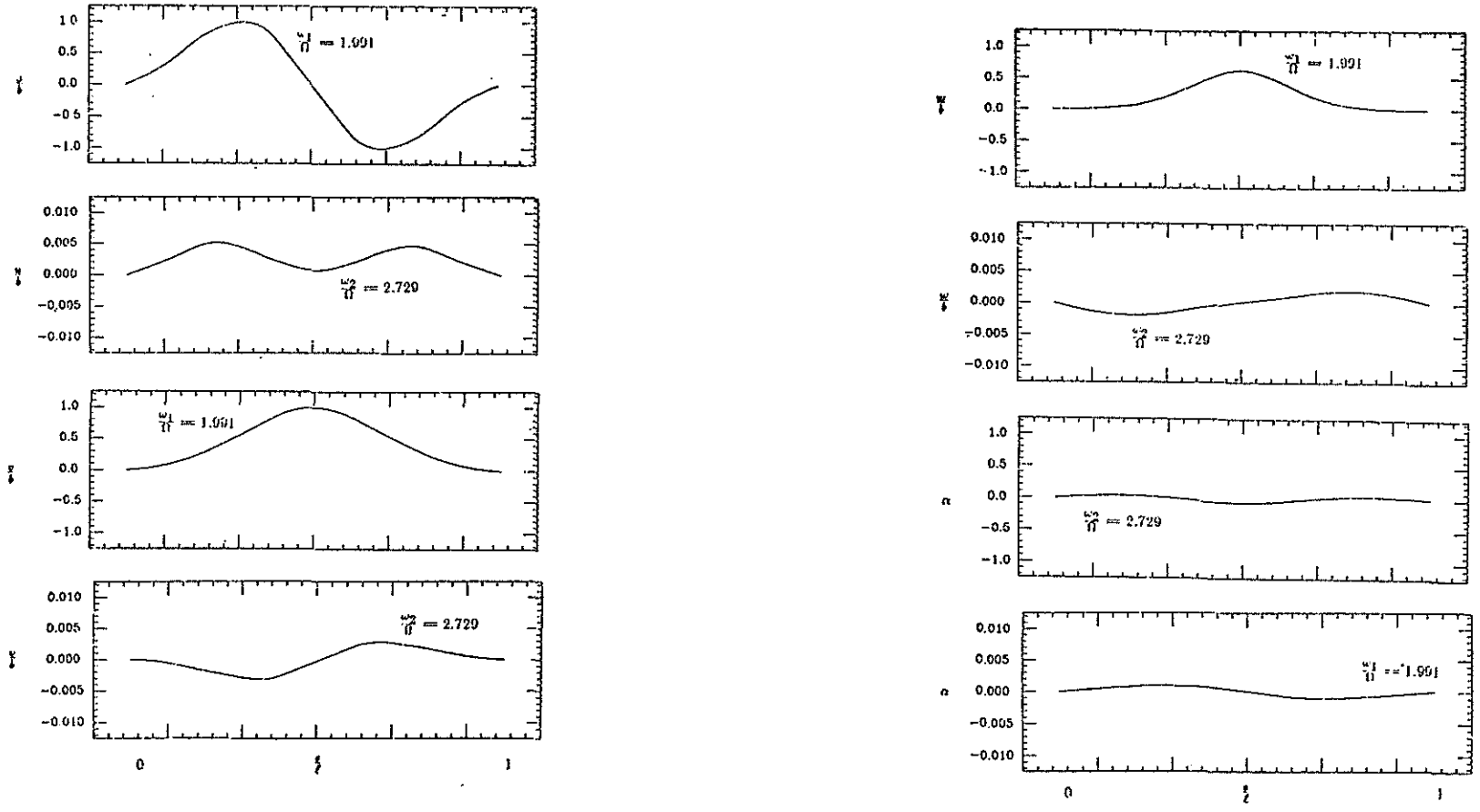

Fig. 9: First two eigenvectors of the case without Coriolis computed at 50 rpm. The components, from left to right and from top to bottom: flatwise bending, chordwise bending, spanwise displacement and torsion. Observe different scales in each situation. Clamped joints and $x_\alpha = -0.1$.

$$\frac{d}{ds}\underline{y} = \underline{G}_{cor}(s;p)\underline{y} \tag{12}$$

where here

$$\underline{G}_{cor}(s;p) = \underline{G}(s;p) + p\underline{C}^*(s) \tag{13}$$

In the Appendix the dimensionless version of the Coriolis-related matrix is presented. The eigenvalue problem is solved as in the previous section. However, in this section, one is dealing with a system with Hermitian character. The new feature is introduced by the skew-symmetric Coriolis-related matrix. For a complete discussion about Hermitian systems and their properties, one is referred to Strang's book on linear algebra[17].

For this particular problem, one may also expect pure imaginary eigenvalues but complex eigenvectors are now generated. In the following examples, normalization of the eigenvectors is made by giving the value (1 + 0j) to the component with maximum amplitude of displacement.

The values of the first two natural frequencies of the pinned blade as the turbine's speed is increased are shown in Fig. 10. Also in Fig. 6, the ratio of these frequencies is plotted, and one then observes that contrary to the case where the Coriolis term was neglected, the ratio of the first two eigenvalues decreases slightly with the spinning rate. This is an indication of the importance of the Coriolis effect on the behavior of the system.

In this analysis the first two natural modes will be called fundamental modes of the troposkien due to similar shape presented by the eigenvectors and the fact that the third natural mode is obviously an harmonic with a greater number of nodes. In Figs. 11 and 12 the first three modes are displayed, respectively, for the

situations with pinned and clamped joints. In both examples $x_\alpha = 0$ and $\Omega = 50$ rpm were assumed. When compared with the case where the Coriolis effect is neglected, these eigenvectores present a higher degree of complexity. All components of the eigenvectors are now different from zero and there is coupling between flatwise and chordwise bending of the blade. Moreover, a phase shift is noticed among these components. Table 2 shows that non-zero components of the fundamental modes when Coriolis was neglected remain in phase when Coriolis is restored. In other words, the pairs flatwise bending-spanwise displacement and chordwise bending-torsion are always in phase. However, in both modes, each individual pair is in quadrature in relation to the other. Since the value of phase depends on the normalization of the eigenvectors, one's attention will be focused only on the difference of phases rather then on the absolute numerical values of the phase angle.

The mechanism of coupling present in the free vibration of the troposkien blade becomes evident when two more cases are analyzed. Figure 13 displays the fundamental modes for the pinned situation at both 20 and 80 rpm for which there is no center of mass offset. One first notices the presence of the following "extra" components of the eigenvectors in the complete eigenvalue problem:

a) chordwise bending in the first mode;
b) flatwise bending in the second mode;
c) torsion in the first mode;
d) spanwise displacement in the second mode.

The second observation concerns the amplitude of these "extra" components. As a general rule, their amplitudes are greater at the higher spinning rate. The third observation is that they are in quadrature in relation to the "primary" components. The common explanation

for all the aforementioned characteristics is based on the Coriolis force, which is proportional to the cross-product $(\dot{\underset{\sim}{\rho}})_R \times \underset{\sim}{\Omega}$. Here, $(\dot{\underset{\sim}{\rho}})_R$ is the relative velocity of the center of mass of the blade cross section and $\underset{\sim}{\Omega}$ is the absolute angular velocity vector of the blade. Figure 14 exhibits the different conditions that occur in the northern and southern hemispheres of the troposkien blade with pinned fixation. $\dot{\underset{\sim}{u}}$, $\dot{\underset{\sim}{v}}$ and $\dot{\underset{\sim}{w}}$ are the components of the velocity vector of the center of mass respectively in the flatwise, chordwise and spanwise directions. The components of the Coriolis force in the same three directions are denoted by $\underset{\sim}{f}_u$, $\underset{\sim}{f}_v$ and $\underset{\sim}{f}_w$. The subscript $(\ )_H$ stands for the horizontal (or radial) component of a vector.

In Figs. 14a and 14b the first fundamental mode is studied. Since this mode is a combination of an antisymmetric flatwise bending and a symmetric spanwise displacement, at a certain instant the velocity vectors are as shown in the two pictures. This configuration criates the Coriolis forces $\underset{\sim}{f}_u$ and $\underset{\sim}{f}_w$ which excite motion in the orthogonal, chordwise direction. Futhermore, the directions of the forces $\underset{\sim}{f}_u$ and $\underset{\sim}{f}_w$ are such that their magnitudes sum in the northern hemisphere and subtract in the southern hemisphere. As a consequence, the resultant chordwise motion is skewed, as one may verify in Figs. 11 and especially 13, where the effect is pronounced at the higher spinning rate (80 rpm).

The second fundamental mode is the matter of study of Fig. 14c. The antisymmetric chordwise bending excites both the flatwise bending and the spanwise displacement of the blade through the Coriolis force $\underset{\sim}{f}_v$ which is in the radial direction. The decomposition of the latter vector in the flatwise and spanwise directions also explains why the spanwise component of the eigenvector is skewed.

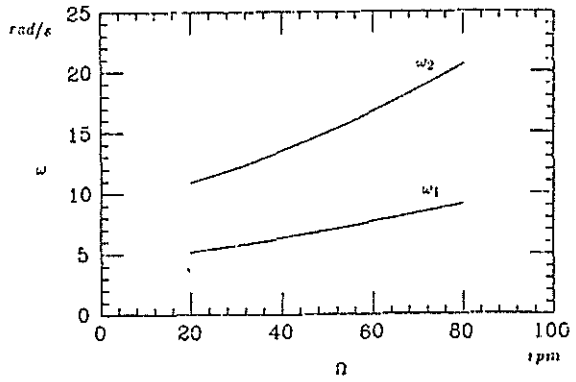

Fig.10: First two natual frequencies as function of the spinning rate. Coriolis effect is included. Pinned joints and $x_\alpha = 0$.

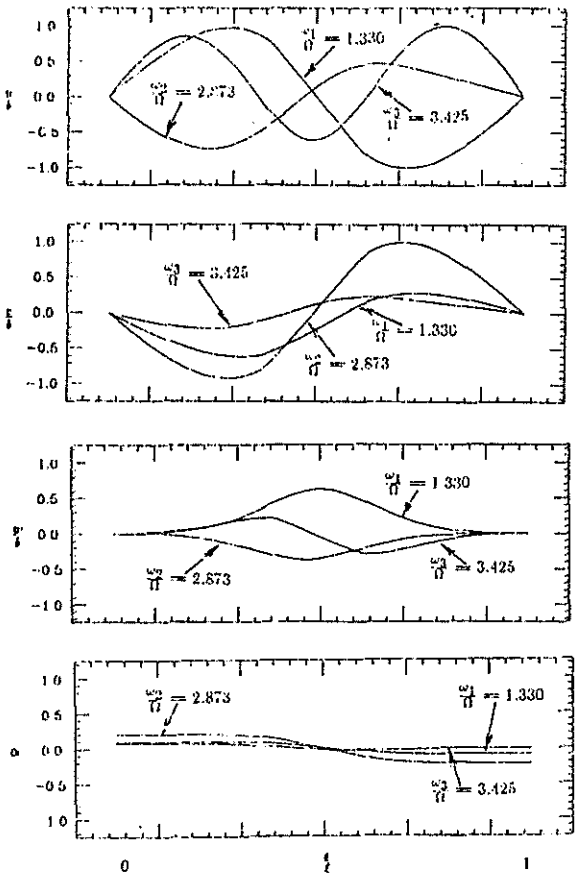

Fig.11: First three eigenvectors at 50 rpm. Coriolis effect is included. The components, from top to bottom: flatwise and chordwise bendings, spanwise displacement and torsion. Pinned joints and $x_\alpha = 0$.

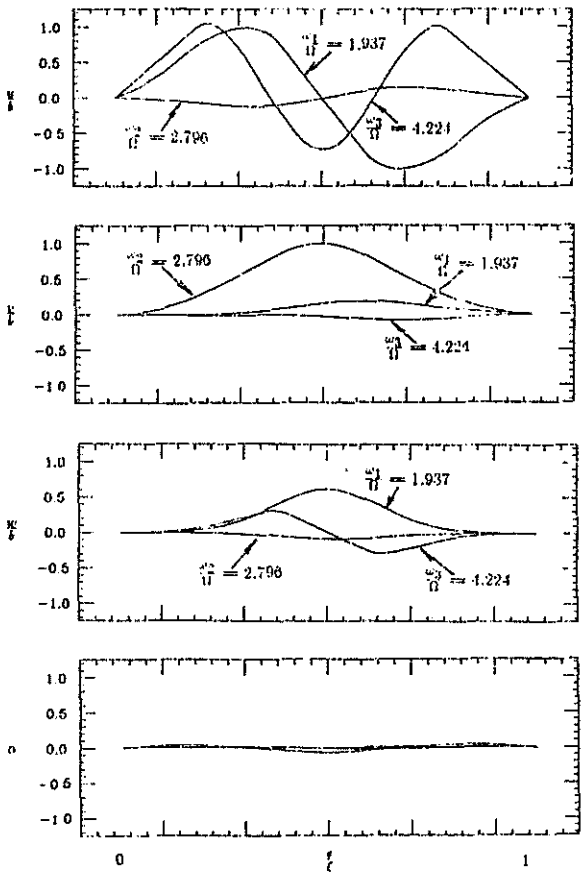

Fig.12: First three eigenvectors at 50 rpm. Coriolis effect is included. The components, from top to bottom: flatwise and chordwise bendings, spanwise displacement and torsion. Clamped joints and $x_\alpha = 0$.

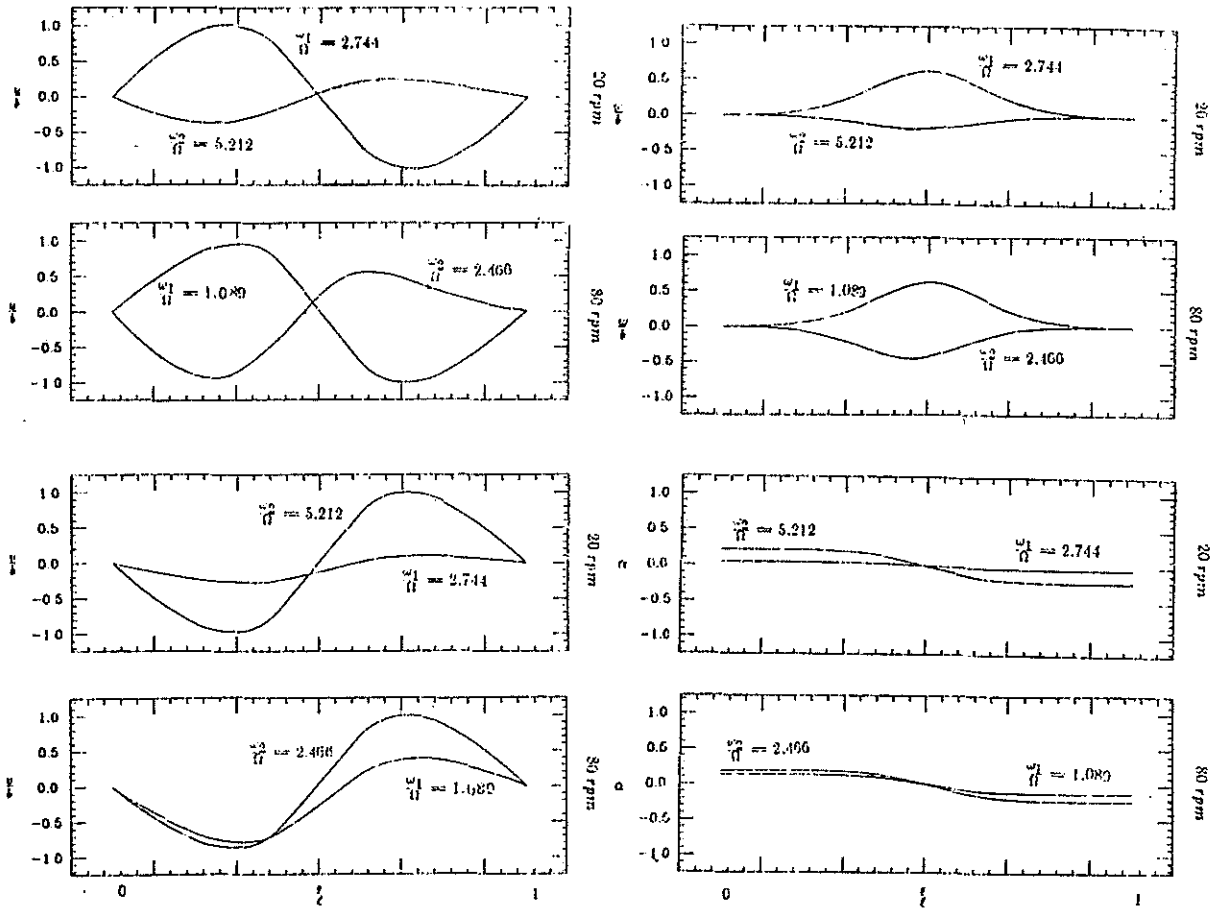

Fig. 13: First two eigenvectors computed at 20 and 80 rpm. Coriolis effect is included. From left to right and from top to bottom: flatwise bending, chordwise bending, spanwise displacement and torsion. Pinned joints and $x_\alpha = 0$.

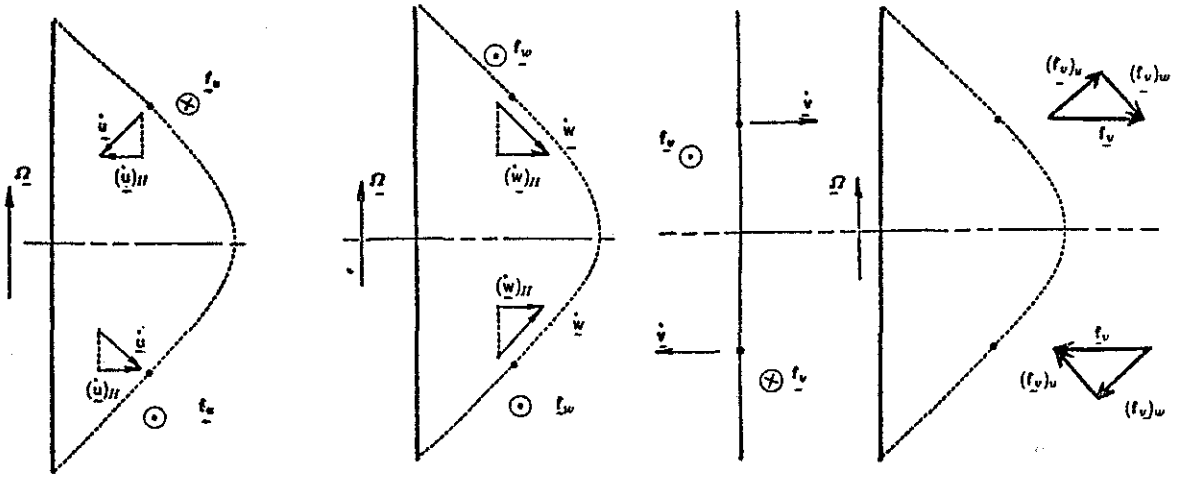

Fig. 14a: The Coriolis coupling: a physical explanation. First mode: flatwise vibration.

Fig. 14b: The Coriolis coupling: a physical explanation. First mode: spanwise vibration.

Fig. 14c: The Coriolis coupling: a physical explanation. Second mode: chordwise vibration.

The differences in phase angle observed in Table 2 may be understood as a consequence of the fact that maximum displacements and maximum velocities are always in quadrature. Since the Coriolis force is directly related to the velocity, the motion that it drives is developed with the same phase difference.

Table 3 presents another interesting point of this analysis. When the center of mass is moved away from the shear center and static unbalance is created in the cross section, the most important change undergone by the system is a slight alteration in the phase angle. Although its mean value remains the same, there is now a characteristic distribution of phase not only among components of the eigenvector, but also among the points along the structure. In other words, each station along the blade span now leads or lags its neighbor by a small phase difference. Here, once more, symmetry is observed: the sum of corresponding phase angles at each station for the cases $x_\alpha = 0.1$ and $x_\alpha = -0.1$ is either 0^0 or 180^0.

6. Summary and Conclusions

The free-vibration characteristics of a blade of a Darrieus turbine curved in a perfect troposkien shape has been studied. The transfer matrix relating the generalized forces and displacements at the two ends of the blade was derived by an integrating-matrix scheme. The physical model is based upon a continuous distribution of both inertia and stiffness properties of the blade. It has been demonstrated the essential role played by Coriolis in the free-vibration eigenvalue problem of the troposkien-curved blade: flatwise, chordwise and torsion vibrations of the structure are all coupled in a three-dimensional motion of the elastic axis about its original position.

7. Acknowledgements

This work has been supported by the following organizations: Conselho Nacional de Pesquisas (Brazil), Instituto de Atividades Espaciais (Brazil), National Aeronautics and Space Administration under Grant NGL-05-020-243 (USA) and the Air Force Office of Scientific Research under Grant 79-0061 (USA).

References:

1) B.F. Blackwell and G.E. Reis: Blade Shape for a Troposkien Type of Vertical - Axis Wind Turbine. Sandia Laboratories Report SLA 74-0154, April 1974.

2) N.D. Ham: Aeroelastic Analysis of a Troposkien - Type Wind Turbine. Sandia Laboratories Report SAND 77-0026, April 1977.

3) N.D. Ham: Flutter of Darrieus Wind Turbine Blades. Proceedings, Wind Turbine Structural Dynamics Workshop, NASA CP-2034/CONF-771148, 1977, pp.77-91.

4) H. Ashley: Use of Asymptotic Methods in Vibration Analysis. Proceedings, Wind Turbine Structural Dynamics Workshop, NASA CP-2034/CONF-771148, 1977, pp. 39-52.

5) H.H. Ottens and R.J. Zwaan: Investigations on the Aeroelastic Stability of Large Wind Turbines. National Aeroespace Laboratory, NLR MP 78014U, Netherlands, April 1978.

6) T.G. Carne et al: Finite Element Analysis and Modal Testing of a Rotating Wind Turbine. Sandia Laboratories Report SAND 82-0345, October 1982.

7) D. Popelka: Aeroelastic Stability Analysis of a Darrieus

Wind Turbine. Sandia Laboratories Report SAND 82-0672, February 1982.

8) G.E. Reis and B.F. Blackwell: Practical Approximations to a Troposkien by Straight - Line and Circular - Arc Segments. Sandia Laboratories Report, SAND 74-0100, March 1975.

9) M.H. Worstell: Aerodynamic Performance of the DOE/Sandia 17-m-Diameter Vertical - Axis Wind Turbine. Journal of Energy, Vol. 5, No. 1, 1981, pp. 39-42.

10) F. Nitzsche: Aeroelastic Analysis of a Troposkien - Type Wind Turbine Blade. Proceedings, International Colloquium on Wind Energy, Brightom, U.K., August 1981. Also NASA CR-165764, July 1981.

11) F. Nitzsche: Aeroelastic Analysis of a Darrieus Type Wind Turbine Blade with Troposkien Geometry. Ph.D. Dissertation, Stanford University, June 1983.

12) F. Nitzsche: A Revised Version of the Transfer Matrix Method to Analyze One-Dimensional Structures. Proceedings, 24th AIAA/ASME/ASCE/AHS Structures, Structural Dynamics, and Materials Conference, Part 2, Lake Tahoe, CA, May 1983, pp 129-136.

13) E.C. Pestel and F.A. Leckie: Matrix Methods in Elastomechanics, Mc Graw-Hill, 1963.

14) W.F. Hunter: Integrating Matrix Method for Determining the Natural Vibration Characteristics of Propeller Blades. NASA TN D-6064, December 1970.

15) S.D. Conte and C. de Boor: Elementary Numerical Analysis, An Algorithimic Approach, 3rd ed., 1980, pp. 120-127.

16) L.L. Lehman: Hybrid State Vector Methods for Structural Dynamic and Aeroelastic Boundary Balue Problems, NASA CR-3591, August 1982.

17) G. Strang: Linear Algebra and its Applications, Academic Press, New York, 1976, pp. 217-231.

Appendix

Dimensionless Free-Vibration Equations in Matrix Form

$$\frac{d}{d\bar{s}}\bar{\underline{Y}} = \underline{\bar{Z}}\,\bar{\underline{Y}} + \lambda\left(\underline{\bar{M}}^{*}\bar{\underline{Y}}_{\beta\theta} + \underline{\bar{C}}^{*}\bar{\underline{Y}}_{\beta} + \underline{\bar{K}}_{D}^{*}\bar{\underline{Y}}\right)$$

$$\bar{\underline{Y}} = \{\bar{Q}_1\ \bar{M}_1\ \bar{Q}_2\ \bar{M}_2\ \bar{\tau}\ \bar{M}_3\ \bar{u}\ \chi_1\ \bar{v}\ \chi_2\ \bar{w}\ \alpha\}^{T}$$

$$\underline{\bar{Z}} = \begin{bmatrix} \underline{\bar{Z}}_{FF} & \underline{\bar{Z}}_{FD} \\ \underline{\bar{Z}}_{DF} & \underline{\bar{Z}}_{DD} \end{bmatrix}$$

$$\underline{\bar{Z}}_{FF} = -\underline{\bar{Z}}_{DD}^{T} = \begin{bmatrix} 0 & 0 & 0 & 0 & -\bar{\kappa}^{(o)} & 0 \\ 0 & 0 & \ell/b & 0 & 0 & -\bar{\kappa}^{(o)} \\ 0 & 0 & 0 & 0 & 0 & 0 \\ -\ell/b & 0 & 0 & 0 & 0 & 0 \\ \bar{\kappa}^{(o)} & 0 & 0 & 0 & 0 & 0 \\ 0 & \bar{\kappa}^{(o)} & 0 & 0 & 0 & 0 \end{bmatrix}$$

$$\underline{\bar{Z}}_{FD} = \frac{\ell}{b}\begin{bmatrix} 0 & & & & \\ & 1/s_\phi & & & \\ & & 0 & & \\ & & & 1/s_\phi & \\ & & & & 0 \\ & & & & & 0 \end{bmatrix}$$

$$\underline{\bar{Z}}_{DF} = \frac{\tau_{max}\,\ell b}{EI_{xx}}\begin{bmatrix} a_1 & 0 & 0 & 0 & 0 & 0 \\ & a_0 & 0 & 0 & -x^{(n)}a_0 & 0 \\ & & a_1 & 0 & 0 & 0 \\ & & & a_3 & 0 & 0 \\ & \text{sym.} & & & a_0 a_2 & 0 \\ & & & & & a_4 \end{bmatrix}$$

$$\underline{\bar{M}}^{*},\ \underline{\bar{C}}^{*},\ \underline{\bar{K}}_{D}^{*} = \begin{bmatrix} \underline{0} & \underline{\bar{M}},\ \underline{\bar{C}},\ \underline{\bar{K}}_{D} \\ \underline{0} & \underline{0} \end{bmatrix}$$

$$\underline{\bar{M}} = \begin{bmatrix} 1 & 0 & 0 & 0 & 0 & -x_\alpha \\ & x_\alpha^2 + r_\alpha^2 & 0 & 0 & x_\alpha & 0 \\ & & 1 & 0 & 0 & 0 \\ & & & 0 & 0 & 0 \\ & \text{sym.} & & & 1 & 0 \\ & & & & & x_\alpha^2 + r_\alpha^2 \end{bmatrix}$$

$$\underline{\bar{C}} = \begin{bmatrix} 0 & 0 & 2s_\phi & 0 & 0 & 0 \\ 0 & 0 & -2x_\alpha c_\phi & r_\alpha^2 s_\phi & 0 & 0 \\ -2s_\phi & 2x_\alpha c_\phi & 0 & 0 & 2c_\phi & 2x_\alpha s_\phi \\ 0 & -r_\alpha^2 s_\phi & 0 & 0 & 0 & r_\alpha^2 c_\phi \\ 0 & 0 & -2c_\phi & 0 & 0 & 0 \\ 0 & 0 & -2x_\alpha s_\phi & -r_\alpha^2 c_\phi & 0 & 0 \end{bmatrix}$$

$$\underline{\bar{K}}_{D}^{*} = \begin{bmatrix} -s_\phi^2 & x_\alpha s_\phi c_\phi & 0 & 0 & s_\phi c_\phi & x_\alpha s_\phi^2 \\ & -x_\alpha^2 c_\phi^2 & 0 & 0 & -x_\alpha c_\phi^2 & -x_\alpha^2 s_\phi c_\phi \\ & & -1 & 0 & 0 & 0 \\ & & & -r_\alpha^2 & 0 & 0 \\ & \text{sym.} & & & -c_\phi^2 & -x_\alpha s_\phi c_\phi \\ & & & & & -x_\alpha^2 s_\phi^2 \end{bmatrix}$$

$$\lambda = \frac{\sigma A\, b\, \ell\, \Omega^2}{\tau_{max}},\quad a_0 = \frac{1}{1 - \frac{1}{a_2}(x^{(n)})^2},\quad a_1 = \frac{EI_{xx}}{b^2\, GA},$$

$$a_2 = \frac{EI_{xx}}{b^2\, EA},\quad a_3 = \frac{EI_{xx}}{EI_{yy}},\quad a_4 = \frac{EI_{xx}}{GI_\alpha}.$$

$$\bar{Q}_{1,2} = Q_{1,2} / \tau_{max},\quad \bar{\tau} = \tau / \tau_{max},\quad \bar{M}_{1,2,3} = M_{1,2,3} / b\,\tau_{max},$$

$$\bar{u},\ \bar{v},\ \bar{w} = u,\ v,\ w / b,\quad \bar{s} = s / \ell,\quad \theta = \Omega t,\quad \bar{\kappa}^{(o)} = \ell\,\kappa^{(o)}.$$

$$\sin\phi = s_\phi,\quad \cos\phi = c_\phi.$$

Table 1

Structural Properties of the 17-meter DOE-Sandia-Alcoa Darrieus

$\ell = 24.1\ m$

$h = 8.5\ m$

$\sigma A = 10.22\ kg/m$

$\Omega = 29.8\text{-}52.5\ rpm$

airfoil section: NACA-0012

$b = 0.2665\ m$

$r_\alpha = 0.1065$

$EI_{xx} = 357.56 \times 10^4\ Nm^2$

$EI_{yy} = 9.0653 \times 10^4\ Nm^2$

$GI_\alpha = 7.1972 \times 10^4\ Nm^2$

$EA = 231.83 \times 10^6\ N$

$GA = 89.316 \times 10^6\ N$

Table 2

Characteristic Phase Angles (in degrees) of theFirst Two Modes of the Pinned Blade at 50 rpm. No CG offset is considered.

mode	coriolis ?	flatwise bending	chordwise bending	spanwise displacement	torsion
1st.	*no*	0°	*	0°	*
	yes	90°	0°	90°	0°
2nd.	*no*	*	0°	*	0°
	yes	90°	0°	90°	0°

*(no such component in this mode)

Table 3

Characteristic Phase Angles (in degrees) of the First Mode of the Pinned Blade at 50 rpm. CG offset is considered.

e/ℓ	x_e	flatwise bending	chordwise bending	spanwise displacement	torsion
0.1	-0.1	87.8743	179.1476	88.1142	-0.0283
	0.0	90	180	90	0
	0.1	92.1257	-179.1476	91.8858	0.0283
0.3	-0.1	87.9446	179.0275	87.9975	-0.2960
	0.0	90	180	90	0
	0.1	92.0554	-179.0275	92.0025	0.2960
0.5	-0.1	89.2625	177.4727	88.0083	-2.3723
	0.0	90	180	90	0
	0.1	90.7375	-177.4727	91.9917	2.3723
0.7	-0.1	-92.0218	1.0384	88.0554	-179.9534
	0.0	-90	0	90	180
	0.1	-87.9782	-1.0384	91.9446	179.9534
0.9	-0.1	-92.0364	0.4515	88.2317	-179.7469
	0.0	-90	0	90	180
	0.1	-87.9636	-0.4515	91.7683	179.7469